Pericytes enable effective angiogenesis in the presence of proinflammatory signals

Tae-Yun Kang[a,b], Federico Bocci[c,d], Mohit Kumar Jolly[e], Herbert Levine[f,1], José Nelson Onuchic[c,d,g,h,1], and Andre Levchenko[a,b,1]

[a]Department of Biomedical Engineering, Yale University, New Haven, CT 06520; [b]Yale Systems Biology Institute, Yale University, New Haven, CT 06520; [c]Center for Theoretical Biological Physics, Rice University, Houston, TX 77005; [d]Department of Chemistry, Rice University, Houston, TX 77005; [e]Centre for BioSystems Science and Engineering, Indian Institute of Science, Bangalore 560012, India; [f]Department of Physics, Northeastern University, Boston, MA 02115; [g]Department of Physics and Astronomy, Rice University, Houston, TX 77005; and [h]Department of Biosciences, Rice University, Houston, TX 77005

Contributed by Herbert Levine, October 7, 2019 (sent for review August 4, 2019; reviewed by Stanislav Y. Shvartsman and Mary N. Teruel)

Angiogenesis frequently occurs in the context of acute or persistent inflammation. The complex interplay of proinflammatory and proangiogenic cues is only partially understood. Using an experimental model, permitting exposure of developing blood vessel sprouts to multiple combinations of diverse biochemical stimuli and juxtacrine cell interactions, we present evidence that a proinflammatory cytokine, tumor necrosis factor (TNF), can have both proangiogenic and antiangiogenic effects, depending on the dose and the presence of pericytes. In particular, we find that pericytes can rescue and enhance angiogenesis in the presence of otherwise-inhibitory high TNF doses. This sharp switch from proangiogenic to antiangiogenic effect of TNF observed with an escalating dose of this cytokine, as well as the effect of pericytes, are explained by a mathematical model trained on the biochemical data. Furthermore, this model was predictive of the effects of diverse combinations of proinflammatory and antiinflammatory cues, and variable pericyte coverage. The mechanism supports the effect of TNF and pericytes as modulating signaling networks impinging on Notch signaling and specification of the Tip and Stalk phenotypes. This integrative analysis elucidates the plasticity of the angiogenic morphogenesis in the presence of diverse and potentially conflicting cues, with immediate implications for many physiological and pathological settings.

angiogenesis | inflammatory | Notch | pericyte

Developmental and physiological processes are frequently guided by diverse, sometimes conflicting cues. For instance, angiogenesis—the growth and morphogenesis of new vascular networks from existing ones—is triggered by the disruption of the local oxygen supply, encoded at the signaling level by a host of secreted factors (1, 2). Angiogenesis also frequently occurs in the presence of proinflammatory stimuli, both acute, as in physiological wound healing, and persistent, as in tumor growth and during various pathologies, including asthma and chronic wounds (3, 4). The proinflammatory signals can have a direct effect on vascular stability, and the initiation and progression of angiogenesis (5–7). The signaling cues in the local microenvironment can also change in time as the oxygen supply is gradually restored and as other concomitant processes, such as resolution of inflammatory response, unfold. Therefore, a proper control of vascular morphogenesis must involve a tight coordination of responses to both proangiogenic and proinflammatory cues. However, despite decades-long research, it is not clear how this coordination is achieved and how it may be misregulated in various pathological settings, including cancerogenesis, leading to the emergence of abnormal structure and function of the vascular beds. In particular, previously reported findings provide conflicting evidence as to whether the local inflammatory response may be proangiogenic or antiangiogenic (5, 7–9). The complexity of the problem is further exacerbated by the intricate organization of vascular and immune systems, involving interaction between multiple cells types within highly organized cellular networks. Thus, new tools and approaches may be needed to address the interplay of distinct environmental and cell-generated cues in regulating angiogenesis or other complex morphogenetic processes.

Angiogenesis has been studied on diverse scales, from molecular networks to tissues, using a very diverse set of techniques. In particular, mimicking angiogenesis in various bioengineered devices by multiple groups has allowed a careful untangling of the basic regulatory mechanisms governing this process (10–12). Many of the inferred mechanisms have been confirmed *in vivo*, justifying the methodology, and leading to its use in tissue engineering efforts and medical interventions. However, a degree of simplification inherent in many of these methods frequently leaves important questions open. Therefore, a continued enhancement of the tissue-modeling technologies is still needed to gain a better understanding of the complex underlying biology. Arguably, these developments can also benefit from computation modeling and theoretical analysis to account for salient features of complex intracellular and intercellular molecular interactions.

A key process underlying angiogenesis is differentiation of endothelial cells (ECs) into diverse phenotypic states, including the so-called Tip and Stalk cells (8, 9, 13, 14). The Tip cells engage in locomotion within a hypoxic tissue leading the growing sprout, while Stalk cells undergo proliferation in coordination with the Tip cell locomotion to ensure the continuity of the growing sprout. These cells can undergo dynamic phenotypic switching, with some

Significance

Angiogenesis is a key physiological or pathological process leading to the growth of new blood vessels from existing ones. This process frequently occurs in the presence of inflammation in the same tissue due to infection-, damage-, or cancer-induced tissue disruption. How the cues controlling angiogenesis and inflammation interact and affect the newly forming vessels is not completely understood. In this study, using a combination of modeling and experiment, we show that a proinflammatory cue can either enhance or suppress angiogenesis, depending on its dose. The change between these 2 opposite roles is very sharp and modulated by accessory cells, called pericytes. These findings can inform our understanding of angiogenesis in different settings, including wound healing and cancer.

Author contributions: H.L., J.N.O., and A.L. designed research; T.-Y.K., F.B., M.K.J., H.L., and A.L. performed research; T.-Y.K., F.B., M.K.J., and A.L. analyzed data; and T.-Y.K., H.L., J.N.O., and A.L. wrote the paper.

Reviewers: S.Y.S., Princeton University; and M.N.T., Stanford University.

The authors declare no competing interest.

Data deposition: All data discussed in the paper will be made available to readers upon request.

[1]To whom correspondence may be addressed. Email: herbert.levine@rice.edu, jonuchic@rice.edu, or andre.levchenko@yale.edu.

This article contains supporting information online at www.pnas.org/lookup/suppl/doi:10.1073/pnas.1913373116/-/DCSupplemental.

First published November 4, 2019.

Stalk cells occasionally replacing the existing Tip cell or forming additional Tip cells and spearheading new branches. These phenotypic states can be induced by proangiogenic factors (15) with the differentiation into distinct states further enhanced in neighboring cells by juxtacrine activation of the Notch signaling pathway (14). As the emerging vessel matures, a lumen forms through a partially understood set of mechanisms, involving cell remodeling and reorganization (1, 16–18). These processes underlying angiogenic morphogenesis can be controlled by both proangiogenic growth factors, such as vascular endothelial growth factor (VEGF), and cytokines associated with inflammation, such as tumor necrosis factor (TNF) (8, 9). Whereas the effects of VEGF are thoroughly explored and well understood, the interplay between VEGF and TNF signaling and the resulting effects of these potentially conflicting cues remain a matter of debate, with little information available about the cross talk of the pathways these ligands can trigger on the molecular level. Furthermore, although supportive mural cells, such as pericytes (PCs) and smooth muscle cells, have been implicated in angiogenesis and maintenance of blood vessels (19, 20), it is not clear how they might modulate the effects of VEGF and TNF, and other relevant cues on ECs.

To address the need for a better, more quantitative understanding of the cross talk between proangiogenic and proinflammatory stimuli, here we report on development of a mesoscale fabrication technique allowing modeling and monitoring of angiogenesis on the single-cell level. This method allows analysis of angiogenesis in the presence of highly controlled prepatterning of ECs and PCs within a collagen matrix, in the presence of diverse combinations of proangiogenic and proinflammatory cues. To account for the experimental findings and to unravel the mechanisms controlling cell differentiation in response to diverse, potentially conflicting cues, we modified and extended a previously developed mathematical model of angiogenesis to account for the effects of TNF and PCs (8). We experimentally validated the model assumptions and predictions, and showed that it can account for various unexpected effects of the complex extracellular milieu. In particular, we demonstrate that the effect of TNF can sharply switch from proangiogenic to antiangiogenic, depending on its concentration and the other environmental inputs. We also show that PCs can modulate the signaling processes activated by proangiogenic and proinflammatory cues, strongly modulating the phenotypic selection at the onset of angiogenesis and rescuing antiangiogenic effects of TNF. These findings can assist in quantitative analysis and control of angiogenesis, particularly in the presence of the inflammatory response, in normal and pathological conditions.

Results

To analyze the effects of different combinations of molecular proangiogenic and proinflammatory cues and of mural cells on angiogenesis, we engineered a biomimetic system allowing precise structuring of an artificial blood vessel, with controlled juxtaposition of layers of ECs and PCs within a collagen gel (see Fig. 1 *A–C* and *SI Appendix*, Fig. S1 and *Materials and Methods* for details). The diameter of the resulting semicylindrical parental vessel was 200 μm, similar to previously published microfabricated 3D angiogenesis models (11, 21). ECs formed a complete monolayer within the engineered parental vessel and produced basement membrane on the abluminal side consistent with correct apicobasal polarity (*SI Appendix*, Fig. S2), forming multiple new lumenized sprouts under proangiogenic conditions described below, as assayed by distribution of dextran-loaded medium from the parental vessel into the growing sprouts (*SI Appendix*, Fig. S3). The unique half-cylinder configuration of this model allowed the positioning of ECs and PCs in the fabrication steps as described in *SI Appendix*, Fig. S1. We next demonstrated the unique feature of this model allowing for precise prepatterning of PCs (or other mural cells) on the abluminal vessel side, during the parental vessel fabrication (*SI Appendix*, Fig. S1). We found that PC assumed elongated morphology with processes, characteristic of their in vivo endothelial coverage (Fig. 1*D*). We note that, unlike other previously described engineered blood vessel models with mural cells (22–25), the major advantage of this newly developed experimental system is a highly controlled juxtaposition between ECs and PCs from the outset of the experiment, without any additional treatment used to recruit PCs onto endothelium from the surrounding gel. The cells were accessible to high-resolution imaging modalities, including confocal microscopy, which was used throughout the experimental analysis presented here. Functionally, one of the effects of PCs is to increase the microvessel stability, which is reflected in lower leakage and permeability to luminal substances. Indeed, we found that the vascular permeability of luminal FITC-dextran was decreased by 40% in the presence of PCs vs. the PC-free version of the system (*SI Appendix*, Fig. S4 *A–D*).

To further investigate the utility of this experimental system for the analysis of angiogenesis, we supplied exogenous proangiogenic and proinflammatory cues (Fig. 1*C*). In particular, we delivered a previously reported (11) proangiogenic mixture by allowing it to diffuse through the collagen gel surrounding the engineered vessel. This mixture contained VEGF supplemented with 40 ng/mL basic fibroblast growth factor (bFGF), 500 nM sphingosine-1-phosphate (S1P), and 75 ng/mL phorbol 12-myristate 13-acetate (PMA). We found that, with or without PCs, within 3 d, this mixture indeed triggered extensive angiogenesis resulting in multiple lumenized sprouts, extending many cell diameters from the parental vessel, frequently with multiple branches (Fig. 1 *E–J*). Notably, if 100 ng/mL TNF was locally supplied in addition to the proangiogenic mixture, in the absence of PCs, the formation of long, lumenized sprouts was completely abolished (Fig. 1 *E* and *H*). Instead, we observed the formation of protrusions primarily consisting of single cells ("minisprouts"), also forming on the abluminal side of the parental vessel wall (Fig. 1*F*). This response suggested that 100 ng/mL TNF had an essentially antiangiogenic effect, perturbing a key aspect of successful luminal sprout formation. Strikingly, this antiangiogenic effect of TNF was completely rescued if the experiment was repeated in the presence of PCs covering the abluminal side of the engineered vessel (Fig. 1 *E* and *J*). Surprisingly, we also found that many of the sprouts forming under these conditions were longer vs. those observed in the absence of TNF, suggesting an additional proangiogenic effect of the TNF–PC combination. On the other hand, the effect of PCs on VEGF-mediated angiogenesis in the absence of TNF was relatively minor, with slight decrease of the number but not the length of the sprouts (Fig. 1 *E* and *I*). Overall, these results supported the experimental assay as a controllable model of angiogenesis. More importantly, our findings revealed a complex control of angiogenesis by multiple cues presented in different combinations, with the effect of TNF strongly modulated by the presence of PCs.

Due to the complex nature of the proangiogenic mixture, we explored whether VEGF signaling alone might interact with the cues provided by TNF and PCs in a fashion similar to that of the whole mixture (Fig. 2 *A–F*). We found that, in the absence of PCs, 100 ng/mL VEGF alone induced a very limited but measurable effect, promoting the formation of single-cell minisprouts (Fig. 2*A*), but not the lumenized longer sprouts enabled by the full mixture. Interestingly, however, we observed that even this limited effect of VEGF was completely abrogated if 100 ng/mL TNF was also supplied to the cell environment (Fig. 2*C*). This result was again suggestive of antiangiogenic effect of TNF, even in the context of a limited proangiogenic phenotype promoted by VEGF. We found that the effect of TNF was again partially reversed in the presence of PCs, leading to a more limited formation of minisprouts (Fig. 2*D*) vs. the effect of VEGF in the absence of PCs and TNF (approximately 2-fold lower minisprout formation) (Fig. 2*B*). The experiments also suggested that PCs without TNF had a more pronounced inhibitory effect on VEGF-induced minisprout formation (number of minisprouts) vs. either sprout or minisprout

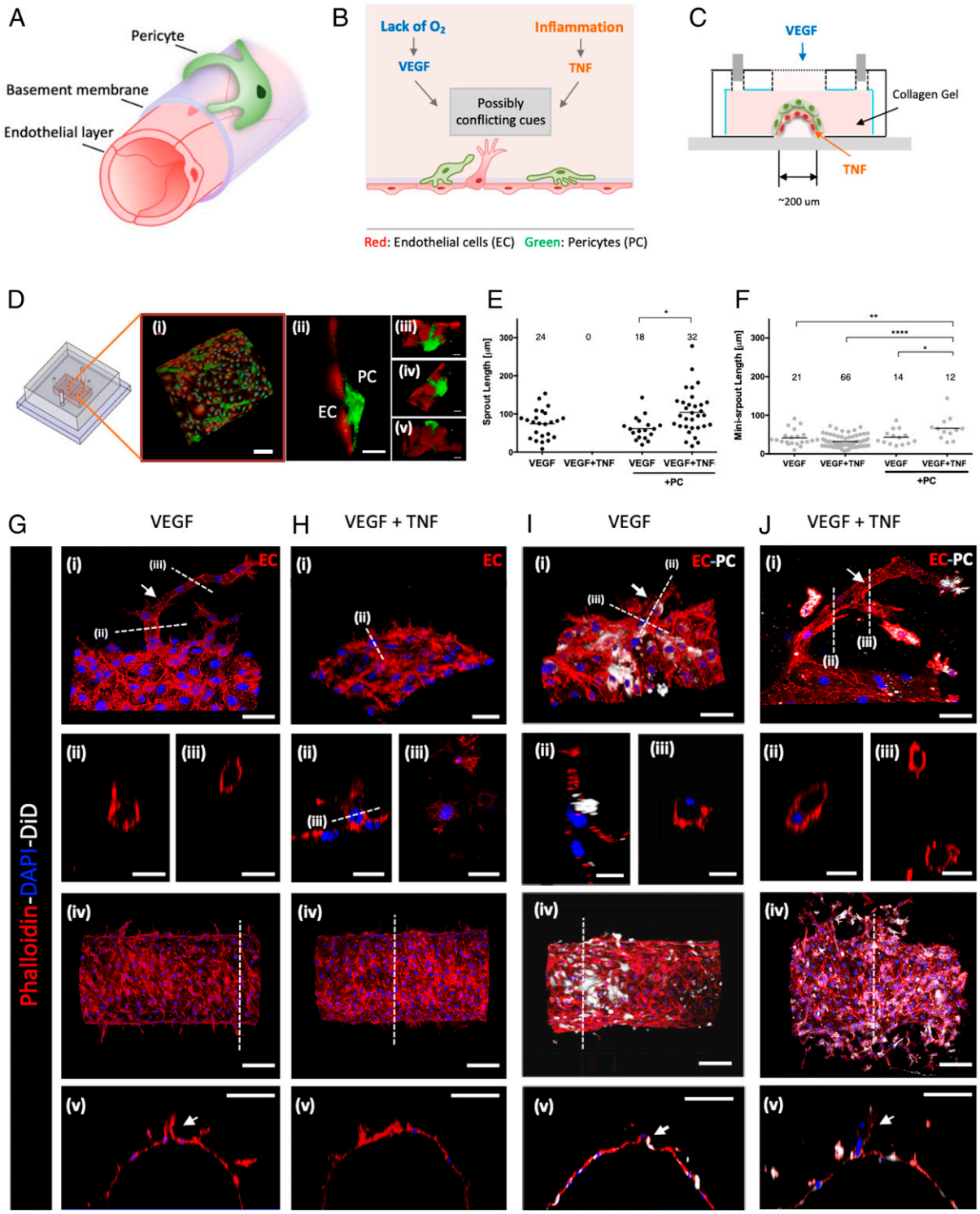

Fig. 1. Three-dimensional angiogenesis model effectuating the interaction between endothelium and PCs. (*A*) Layered structure of a capillary vessel: endothelium, basement membrane, and PCs. (*B*) Schematic description of angiogenesis costimulated by cues from inflammation and ischemic tissue. This study focuses on how those possibly conflicting cues control angiogenesis in multicellular vessel structure. (*C*) Schematic diagram of 3D angiogenesis model mimicking the organization of capillary vessel embedded in collagen type I. (*D*) Confocal images of ECs (red) and PCs (green): (*i* and *ii*) ECs formed a monolayer on the channel, and PCs were covering the endothelium in close proximity. (Scale bar, 100 μm.) (*iii*–*v*) Basal sides of ECs and PCs were facing each other. (Scale bar, 20 μm.) Quantified lumenized sprouts (*E*) and single-cell–sized minisprouts (*F*) from angiogenesis assay on the 3D angiogenesis model. Data were acquired from 4 positions with 2 independent experiments for each condition. $*P < 0.05$, $**P < 0.01$, $***P < 0.001$, and $****P < 0.0001$. Confocal images of lumenized sprouts formation in response to gradient of VEGF (*G*), single-cell–sized minisprouts formation in response to gradient of VEGF and local TNF (*H*), shorter sprouts in response to gradient of VEGF in the presence of PC (*I*), the rescued sprout formation in response to gradient of VEGF and local TNF in the presence of PCs (*J*). Actin filaments of ECs and PCs were stained with phalloidin (red), and PCs were prelabeled with DiD (white). Nucleic acid was stained with DAPI (blue). The white arrows in *G* (*ii* and *iii*), *I* (*ii* and *iii*), and *J* (*ii* and *iii*) indicate sprouts with hollow lumens. (Scale bar: 50 μm in *i*, 25 μm in *ii* and *iii*, 100 μm in *iv* and *v* of *G*–*J*.) Mixture medium was used as a basal medium for all samples. Samples were treated with VEGF and TNF for 3 d.

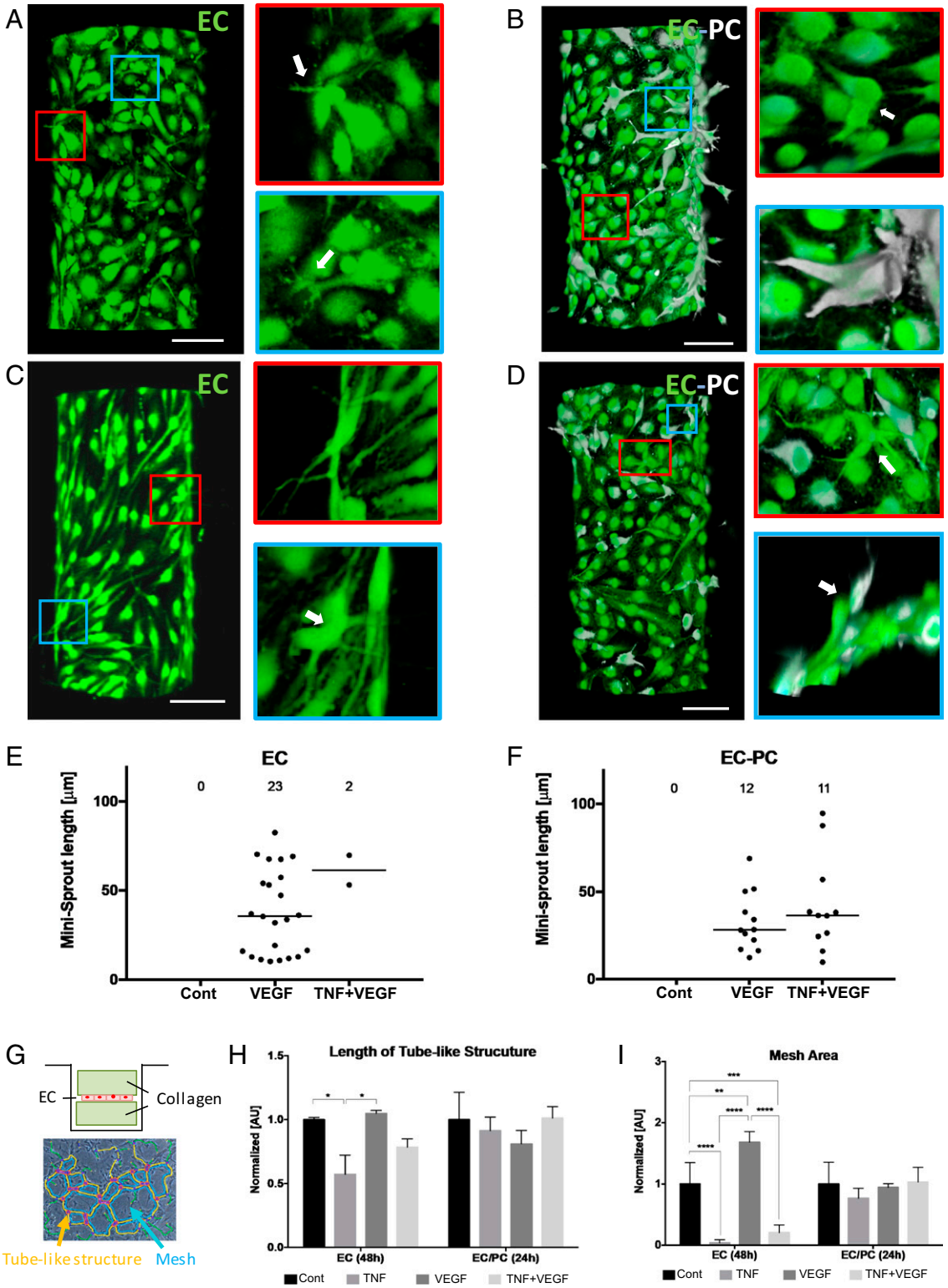

Fig. 2. Interplay of TNFα and VEGF on initiation of angiogenesis and its alteration by PCs. Representative images of minisprouts formation and cell migration induced by VEGF without (*A*) and with (*B*) PCs. Inhibited minisprouts formation by TNF without PCs (*C*) and rescued minisprouts formation by PCs (*D*). GFP-tagged ECs (green) and DiD-prelabeled PCs (white). (Scale bar, 100 μm.) The white arrows indicate single-cell minisprouts, which are the limited angiogenic response in normal growth medium without any supplement. Quantification of minisprouts formation without (*E*) and with (*F*) PCs. Data were acquired from 4 positions with 2 independent experiments for each condition. Samples were treated with VEGF and TNF for 3 d. (*G*) Experimental setup for vasculogenesis assay. Endothelial monolayer was cultured between 2 collagen layers, and TNF and VEGF were added with normal culture medium. Total length of tube-like structure (*H*) and mesh area (*I*) were quantified from *SI Appendix*, Fig. S5. Error bars, SD ± mean of experiment values obtained in triplicate. $*P < 0.05$, $**P < 0.01$, $***P < 0.001$, and $****P < 0.0001$.

formation induced by the full mixture (Fig. 2 *E* and *F*). Overall, these results supported the rescue effect that PCs can have on the antiangiogenic TNF signaling, even in the presence of a weak proangiogenic signal leading to incomplete sprout formation.

We also performed a more traditional vasculogenesis-mimicking assay relying on culturing cells being "sandwiched" between 2 slabs of collagen gel (Fig. 2*G*). As expected, this cell culture method resulted in the characteristic mesh networks indicative of EC self-organization, thought to be reflective of conditions also leading to the vascular bed formation in vivo (Fig. 2*G* and *SI Appendix*, Fig. S3 *A–H*). We again found that the formation of these networks was significantly perturbed by TNF and that this inhibitory effect was rescued by the presence of PCs (Fig. 2 *H* and *I*).

Given the observed effects of TNF and PCs, we next investigated the molecular mechanisms of cross talk between proangiogenic and antiangiogenic cues and their modulation by PCs. Successful angiogenesis relies on a coordinated differentiation of ECs in the parental vessel into the Tip and Stalk phenotypic states. This process is regulated by activation of the Notch-mediated signaling, serving, as in many other differentiation contexts, to stabilize distinct cell fates in adjacent cells. Two Notch-ligands have been strongly implicated in regulation of Notch activity during angiogenesis: Delta-4 (Dll4) and Jagged-1 (Jag1) (8, 9, 14). Furthermore, VEGF and TNF can induce the expression of Dll4 and Jag1, respectively (9, 26). We therefore investigated how the signaling networks specific to VEGF and TNF might interact with each other in the presence or absence of PCs. To enable this analysis, we simplified the experimental system by culturing ECs as a monolayer, both in isolation and in coculture with PCs (Fig. 3*A*). Two types of coculture were used. In the first, the PCs were cultured on a porous membrane within an insert that was within the same culture medium as the ECs, enabling spatial separation of the heterotypic cells, but also a possibility of paracrine interactions between them (EC/PC coculture). In the second, the ECs and PCs were cocultured on 2 sides of the same porous membrane, which enabled both contact-mediated and paracrine interactions (EC–PC coculture). Indeed, we observed ECs and PCs making contact through the 0.4-μm pores and forming N-cadherin–rich junctions in EC–PC coculture (Fig. 3*B*). The results in the above coculture experiments were contrasted with those from an endothelial monolayer monoculture experiments (EC culture), used as a control condition.

We then evaluated the signaling responses to TNF or VEGF alone, or the mixture of these signals. In particular, we analyzed the phosphorylation of NF-κB and Erk at 10 min following the stimulation (the time at which these pathways display a high acute activation), as these pathways are both implicated in specific responses to these ligands, and as mediating Jag1 and Dll4,

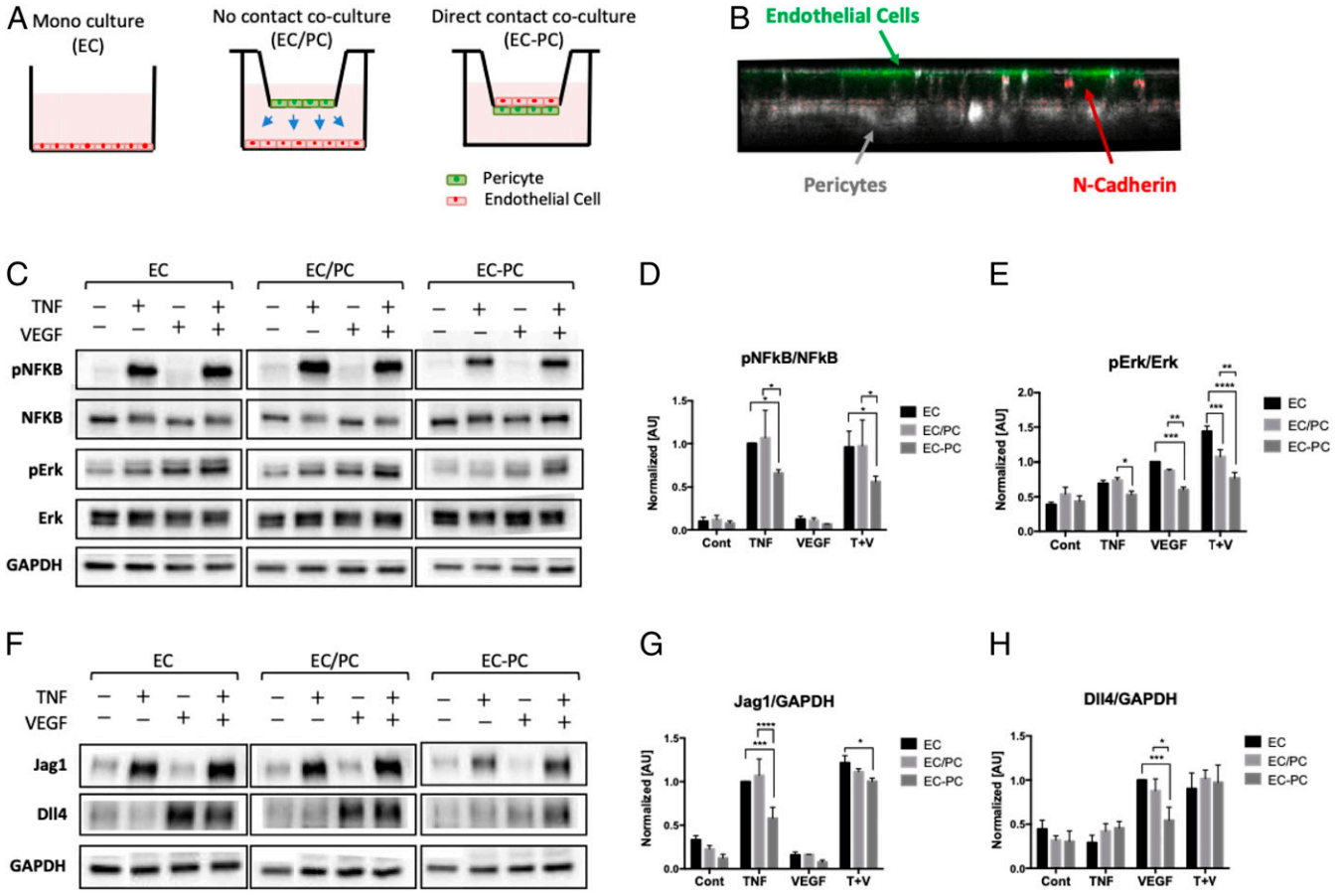

Fig. 3. Inhibition of TNFα- and VEGF-mediated signaling pathways on endothelium in a PC contact-dependent fashion. (*A*) Experimental setup for monoculture (EC), no contact coculture (EC/PC), and direct contact coculture (EC–PC) of ECs and PCs using Transwell inserts. (*B*) ECs (green) and PCs (white) sitting across a permeable membrane. ECs and PCs are making N-cadherin (red) adhesion through pores of the Transwell membrane. (*C*) Phosphorylation levels of TNF and VEGF downstream targets analyzed by Western blots. The bar graphs of pNFkB/NFkB (*D*) and pErk/Erk (*E*) were quantified from blot images ($n = 3$). (*F*) Notch ligand Jag1 and Dll4 expression analyzed by Western blots. The bar graphs of Jag1/GAPDH (*G*) and Dll4/GAPDH (*H*) were quantified from the blot images ($n = 3$). PCs downregulated the downstream of VEGF and TNF in ECs, in a cell contact-dependent fashion. Error bars, SD ± mean of experiment values obtained in triplicate. $^{*}P < 0.05$, $^{**}P < 0.01$, $^{***}P < 0.001$, and $^{****}P < 0.0001$.

respectively. We found that NF-κB was indeed potently activated by TNF, whereas VEGF primarily activated Erk, under all conditions (Fig. 3 *C–E* and *SI Appendix*, Fig. S6 *A* and *B*). Furthermore, the effect of the combination of VEGF and TNF was additive, suggesting a limited cross talk between the signaling pathways downstream of the receptors. We then investigated the effect of PCs on the signaling outcomes. In the EC/PC coculture, we found that PCs had no significant effect on the phosphorylation of the signaling molecules (Fig. 3 *C–E*), with a possible exception of JNK (*SI Appendix*, Fig. S6 *A* and *B*). On the other hand, in the EC–PC coculture, there was a strong and highly significant inhibitory effect on all signaling molecules (Fig. 3 *C–E*). These results suggested that PCs inhibit signaling by both VEGF and TNF in a contact-dependent fashion.

We then explored if these short-term signaling effects could be reflected in the longer term changes in the expression levels of Jag1 and Dll4. We found, as expected, that, at 16 h following exposure to signaling inputs, VEGF specifically induced an increased expression of Dll4, whereas TNF enhanced the expression level of Jag1 (Fig. 3 *F–H*). We further observed that a combination of these ligands induced the expression of Dll4 and Jag1 to levels induced by each of the corresponding signaling inputs alone, again suggesting a very limited cross talk between the signaling pathways. We also again did not observe a significant effect of PCs on expression of these 2 molecules in the EC/PC coculture (Fig. 3 *F–H*). However, in the EC–PC coculture case, we found a significant down-regulation of Jag1 and Dll4 in response to TNF and VEGF inputs, respectively (Fig. 3 *F–H*). Interestingly, despite the additive signaling effect of the 2 ligands, the influence of PCs on the combined action of TNF and VEGF in the EC–PC coculture was much more muted but has nevertheless resulted in a significant reduction of Jag1 levels vs. the control case (Fig. 3 *F–H*). Overall, these results suggested that PCs may down-regulate the VEGF- and TNF-induced expression of Dll4 and Jag1 in ECs, in a cell contact-dependent fashion, in a manner consistent with the effects of PCs on the signaling pathways triggered by these proangiogenic and antiangiogenic factors. However, these results also raised the question of why the effect of PCs in the EC–PC coculture on expression of Dll4 was not significant. More generally, it was not clear how these molecular interactions might quantitatively translate into angiogenic outcomes. We thus next explored these questions and the angiogenic response more generally through a combination of mathematical modeling and experimental analysis in the 3D angiogenesis model.

To further investigate the possible interplay between TNF and VEGF signaling in the presence of PCs and its effect on the expression of Jag1 and Dll4, and, ultimately, angiogenesis, we developed a mathematical model, partially based on a previous study (8). We note that this model, as any other model, was a simplification of a much more complex process. In particular, the focus on the model was not on the consistently present components of the cell microenvironment, e.g., various components of the proangiogenic mixture or the chemical and mechanical cues emerging from the extracellular matrix of luminal medium. Rather, the model was focused on the variable environmental components, including VEGF and TNF. Fig. 4*A* shows the schematic diagram describing the interactions between Notch, VEGF, and TNF signaling. VEGF and TNF are treated as extracellular input signals, whereas the intracellular signaling networks consist of 3 interconnected modules: the Notch module, the VEGF response module, and the TNF response module. The Notch module models signaling due to the engagement of the Notch receptor by the Dll4 and Jag1 ligands, transduced by the cleaved Notch Intracellular Domain (NICD). The VEGF and TNF modules describe lumped signaling pathway activations in response to each of these ligands. These modules interact with the Notch module through a cross-talk mechanism as described below (26). First, TNF induces the expression of Jag1 by activating NF-κB. Moreover, NCID can transcriptionally inhibit the expression of the VEGF receptor (VEGFR2) (27, 28), whereas activated VEGF module (AVEGF) induces the expression of Dll4. Finally, according to the published studies (28), and as captured by the previous model (8), activated Notch module can suppress Dll4 transcription and induce Jag1 transcription in the same cell. These interactions have been modeled as a series of ordinary differential equations, as described more in detail in *SI Appendix*, *Mathematical Modeling*. Finally, we also introduced the effect of PCs into the model by specifying the degree to which these cells can suppress the activation of Dll4 and Jag1 (Fig. 4*B*), based on the experimental data above (Fig. 3). Since the key phenotypic outcome regulated by these signaling pathways and controlling the initiation and progression of angiogenesis is the specification of the Tip and Stalk cells in adjacent cells, we further implemented the model on the scale of 2 adjacent cells, focusing, in particular, on whether the signaling interactions would result in differentiation of these model cells into the divergent phenotypic states.

Analysis of the model revealed that cell exposure to combinations of VEGF and TNF concentrations resulted in diverse phenotypic responses, including the Tip phenotype (classified according to high levels of VEGFR and Dll4), the Stalk phenotype (low VEGFR, Dll4), as well as a less frequently discussed hybrid Tip/Stalk phenotype (8) with intermediate levels of VEGFR, Dll4 (*SI Appendix*, Figs. S7–S9). These results were summarized as a "phenotypic phase diagram" (Fig. 4*C*). This diagram revealed that the degree of cellular differentiation expressed as the ratio of VEGFR activation levels in 2 adjacent cells increased gradually with the increasing VEGF input. This outcome was mediated by a gradual change in VEGFR activity in each of the cells (Fig. 4*D*). Interestingly, the model also predicted a putatively proangiogenic role of TNF, through promoting the Tip fate outcome, up to the threshold level (Fig. 4*E*), consistent with the observations above (Fig. 5*B*). When the TNF dose exceeded this threshold level, there was a very abrupt abrogation of the cell differentiation, leading to an undifferentiated (or "hybrid Tip/Stalk") state corresponding to similar levels of VEGFR activation in both of the modeled cells. This undifferentiated state of 2 neighboring cells was expected to disrupt effective angiogenesis, although individual cells might still adopt phenotypes promoting migration or proliferation, as described more in detail below. Overall, the model predicted that TNF-induced Notch–Jag1 signaling initially stabilizes the Tip phenotype, putatively leading to proangiogenic responses at low doses, but prevents Notch-Dll4–driven Tip–Stalk differentiation, and thus is antiangiogenic at higher doses, after exceeding a sharply defined threshold. These findings were consistent with the experimentally observed antiangiogenic effect of TNF at high doses (Figs. 1 *E–J* and 2 *A–F*) but left open the question of whether lower doses of TNF, below the predicted threshold, would indeed be proangiogenic, as predicted by the model.

Finally, we investigated the effect of PCs on the modeling outcomes. In the case of dense coverage, allowing both model cells to receive the PC input (2 bound cells in Fig. 4*G*), we found that, for experimentally defined parameters, PCs could completely rescue the antiangiogenic effect of high TNF doses (Fig. 4 *C* and *F*). Since PCs make structurally complex contacts with ECs, even the complete coverage might result in differential degree of PC input. We thus explored the effect of a graded PC coverage, finding that it resulted in a progressive shift of the threshold boundary formed by the critical TNF inputs for different VEGF levels, the coverage increased (Fig. 4 *G* and *H*). Strikingly, if the coverage was incomplete, so that only 1 cell in the cell pair was in contact with the PC (1 bound cell in Fig. 4*G*), the effect of graded PC input was much more pronounced, with only a moderate change of this input leading to a strong shift of the TNF threshold and thus more pronounced PC-mediated rescue effect (Fig. 4*I*).

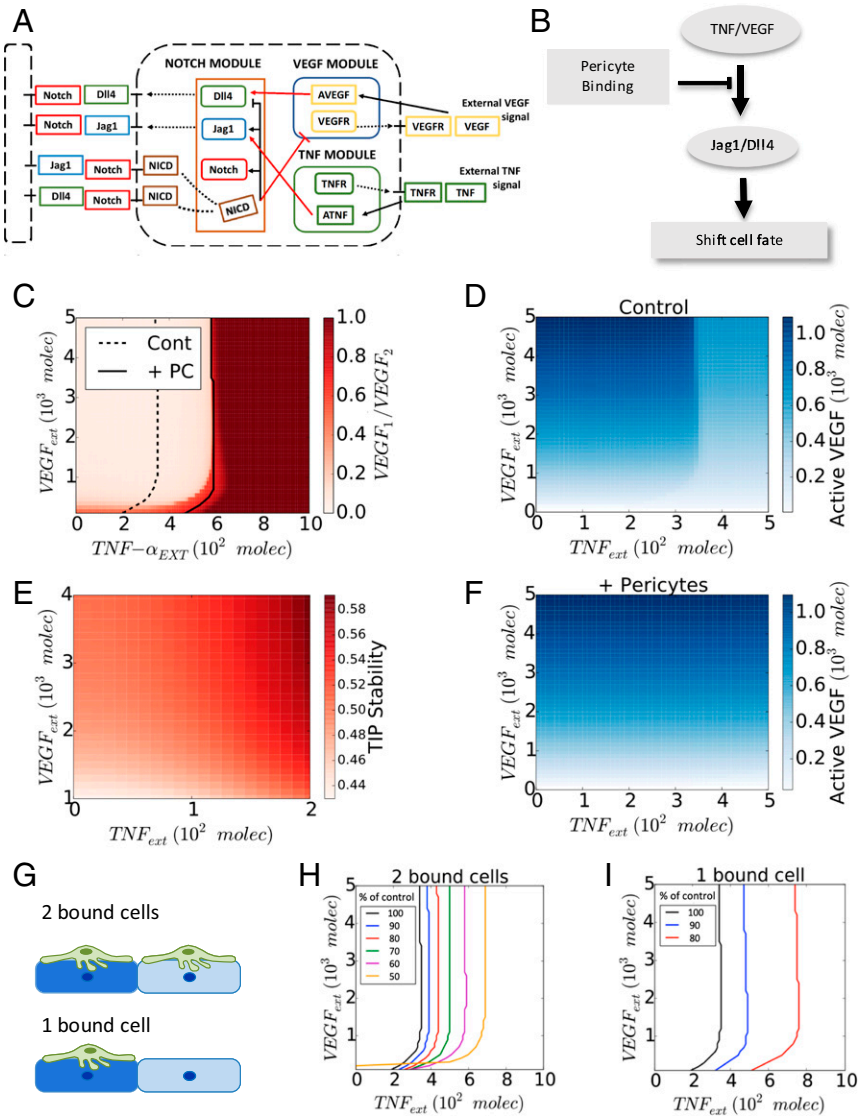

Fig. 4. PCs shift the transition line between 2 distinct Tip–Stalk fate decision phases of ECs. (*A*) Schematic diagram of the connections between Notch, VEGF, and TNF signaling. The red arrows highlight the cross talk between the 3 components. Notch intracellular domain (NICD) transcriptionally inhibits VEGF receptor (VEGFR), while activated VEGF signaling (AVEGF) induces Dll4. Similarly, activated TNF signaling (ATNF) induces Jagg1. (*B*) Schematic summary of the role of PC binding on Notch signaling pathway and cell-fate decision in angiogenesis. (*C*) Phase diagram of the relative VEGF activity ($VEGF_1/VEGF_2$) in a 2-cell system for different levels of external TNF (*x* axis, TNF_{ext}) and VEGF (*y* axis, $VEGF_{ext}$) signal. PCs slightly modify the action of external VEGF while inhibiting completely the effect of external TNF. (*D*) Heatmap of the level of active VEGF signaling in 1 of the 2 cells in bare endothelium. (*E*) The stability of the Tip cells by external TNF and VEGF (see *SI Appendix*, Fig. S10 for the details). (*F*) Heatmap of the level of active VEGF signaling in 1 of the 2 cells in the presence of PCs. (*G*) Description of 2 bound cells system and 1 bound cell system. Green cells and blue cells indicate PCs and ECs, respectively. The dark and light blue shades imply cell fate differentiation between adjacent cells. Variation of the transition line upon the strength of inhibitory effect of PCs in 2 bound cells system (*H*) and 1 bound cell system (*I*). As the value of p decreases, the transition line shifts further toward higher external TNF signal. The value of p represents the percentage of Dll4 and Jag1 expression reduced by PCs.

Indeed, Notch-driven cell differentiation emerges from dynamical competition among neighbors, and partial PC coverage could potentially provide an additional bias to cell fate decision (29). We then sought to validate these predictions in the experimental setting modeling angiogenesis in various defined combination of VEGF and TNF ligands described in Fig. 1.

One of the model predictions is that TNF, by inducing Jag1, indirectly suppresses Dll4 expression, consistent with prior literature reports (9), which may also account for its negative effect on Tip vs. Stalk differentiation beyond a threshold level. This prediction also suggests that a combination of VEGF and TNF would exert positive and negative effects on Dll4 expression, respectively. Therefore, although both VEGF and TNF signaling may be attenuated by PCs, when these molecular factors are present simultaneously, their attenuations can essentially cancel each other and thus PC input might not strongly affect Dll4 expression, as indeed observed experimentally above (Fig. 4 *C–E* and *SI Appendix*, Fig. S8 *A–C*). On the other hand, the negative PC effect on the expression of Jag1 would be specific to attenuation of TNF signaling only and thus would still be predicted to also occur under the costimulation conditions, again in agreement with the experimental data (Figs. 1 *E–J* and 2 *A–F*).

A more stringent test of the model can be provided by experimental exploration of the model space represented in the "phase diagram" shown in Fig. 4*C*. To accomplish this, we exposed the cells in the 3D angiogenesis assay described in Fig. 1 to 6 combinations

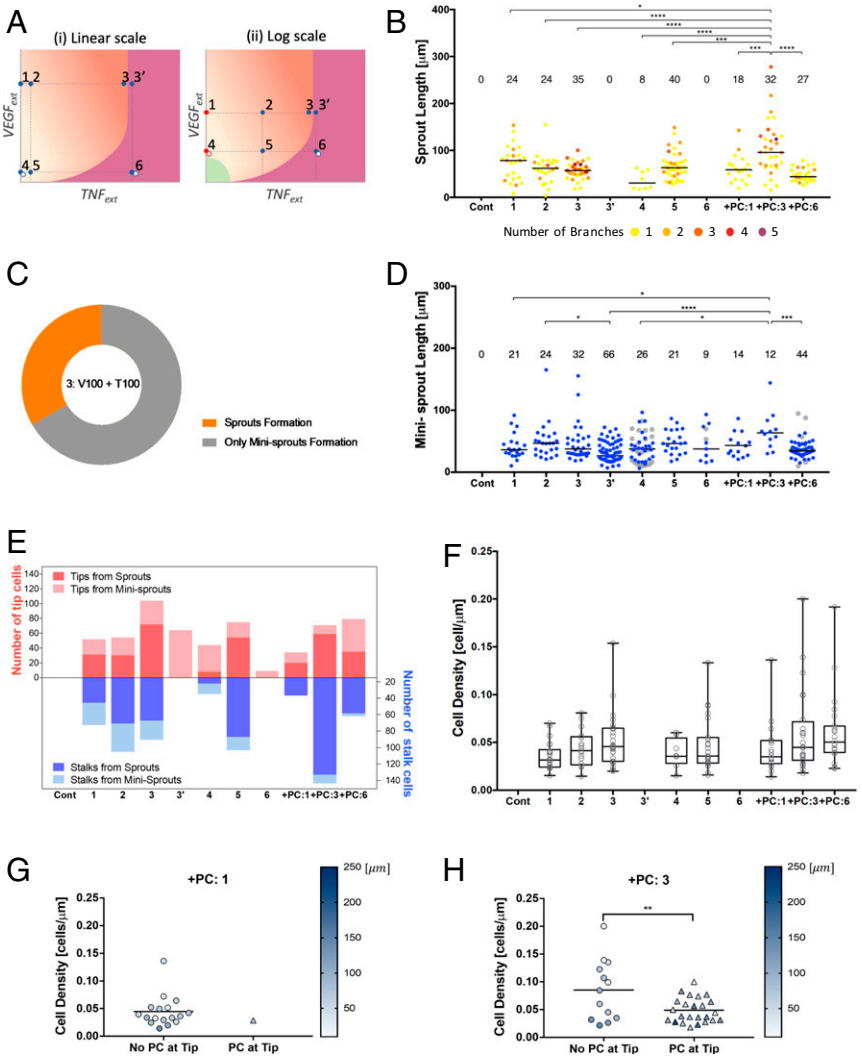

Fig. 5. PCs binding substantially improves the stability of the Tip/Stalk differentiation process under inflammation. (*A*) Conceptual phase diagram of settled Tip–Stalk (T–S) decision phase (pale orange) and stalled Tip/Stalk–Tip/Stalk (T/S–T/S) decision phase (deep orange) displayed in linear scale (*i*) and logarithmic scale (*ii*). Points 1 and 4 are indicated with red dots in logarithmic scale due to the zero value of VEGF. The gray dots at points 4 and 6 represent the conditions presumably corresponding to those in Fig. 2. The condition of points 3 and 3′ is the same, but they are marked separately according to contradictory outcomes. (*B*) Quantification of lumenized sprout formation according to TNF and VEGF concentrations specified in Table 1. Color codes from 1 to 5 of sprouts indicate the number of branches. (*C*) Two possible and conflicting outcomes at point 3 from 6 independent experiments. The data from each experiment is presented in *SI Appendix*, Fig. S10. (*D*) Quantification of single-cell–sized minisprouts formation according to TNF and VEGF concentrations specified in Table 1. Data from Fig. 2 *E* and *F* are displayed at 4, 6, +PC:6 with gray dots. (*E*) Quantification of the number of leading tip cells and following stalk cells from newly lumenized sprouts. Escalating TNF levels were initially proangiogenic, but there was a complete abrogation of the formation of lumenized sprouts beyond a critical TNF level (point 3′ and point 6). This antiangiogenic effect of TNF was completely rescued if the experiment was repeated in the presence of PCs (+PC:3 and +PC:6). (*F*) Cell density of tubes, which is calculated by dividing the number of cells consisting a sprout by its length. Increase of cell density along with TNF level represented the stalk cell growth promoted by TNF, resulting in thicker sprout formation. Cell density of +PC:1 condition (*G*) and +PC:3 condition (*H*), which was separated upon the presence of PCs at the tip of sprouts. Color scale represents the length of sprout. PCs maintaining physically close contact with tip cells guided ECs to form longer and thinner sprouts. Sprouts of +PC:6 were too short to differentiate PCs at tip and stalk. Data were acquired from 4 positions with 2 independent experiments for each condition. $*P < 0.05$, $**P < 0.01$, $***P < 0.001$, and $****P < 0.0001$. Samples were treated with VEGF and TNF for 3 d.

of different concentrations of VEGF (in the presence of the proangiogenic mixture components, assumed to be constant in the model and kept constant in experiment) and TNF, in the presence or absence of PCs (Table 1). To provide a quantitative assessment of the angiogenic response (*SI Appendix*, Fig. S11), we evaluated several parameters of the emerging sprouts. They included the number of branches, the sprout length (in the case of several branches, we recorded the longest distance from a branch tip of the sprout to the root of the sprout connecting it to the parental vessel), the lumenized and multicellular nature of the sprouts, as well as the number of cells which have been assigned the Tip and Stalk fates (see *Materials and Methods* for details of this analysis). Using these metrics, we found the following.

Without TNF and in the absence of PCs, in agreement with the mathematical model, the angiogenic response increased with the increasing VEGF dose, yielding a greater number of lumenized sprouts, which were longer and more branched (points 1 vs. 4 in Fig. 5 *A* and *B*). Also, in agreement with the mathematical model predictions, at each VEGF dose, escalating TNF levels were initially proangiogenic, increasing the number and branching of sprouts, as well the Tip cell formation (cf. points 1, 2, 3, and 4, 5, and Fig. 5*E*). However, also agreeing with the model prediction,

Table 1. TNF and VEGF concentration used in 3D angiogenesis model

	Cont	1	2	3	4	5	6
VEGF, ng/mL	0	100	100	100	10	10	10
TNF, ng/mL	0	0	10	100	0	10	100

there was a complete abrogation of the formation of lumenized sprouts beyond a critical TNF level. The strikingly abrupt nature of this threshold phenomenon was underscored when cells were exposed to the combination of 100 ng/mL TNF and 100 ng/mL VEGF (the maximal amounts for both ligands used here). This was the only combination of inputs that provided 2 types of outcomes, varying from experiment to experiment. In 2 of 6 independent experiments (Fig. 5*C* and *SI Appendix*, Fig. S12*A*), there was an extensive formation of highly branched sprouts (point 3 in Fig. 5*A*), whereas in 4 out of 6 independent experiments (Fig. 5*C* and *SI Appendix*, Fig. S12*A*), the lumenized sprout formation was completely shut down (denoted as point 3′ in Fig. 5*A*). This result indicated that this combination of TNF and VEGF inputs led to a divergent outcome due to being very close to the very sharp threshold separating the proangiogenic and antiangiogenic effects of TNF, with the outcome defined by a slight variation of experimental conditions. This allowed us to connect this experimental point with the phenotypic phase diagrams shown in Fig. 4 *C* and *D*, indicating the position of the threshold levels. The model also predicted that the threshold TNF levels would shift slightly to the lower concentration values for lower VEGF inputs (Fig. 4 *C* and *D*). In agreement with this prediction, when the VEGF concentration was lowered to 10 ng/mL, while keeping TNF levels at 100 ng/mL (point 6 in Fig. 5*A*), we observed an unambiguous and complete inhibition of lumenized sprouting in all experimental repeats (Fig. 5*B*). We noted that, at the TNF levels exceeding the threshold, there was still formation of single-cell minisprouts (Fig. 5*D*) and Tip cells (Fig. 5*E*), which, however, were not supported by sprout growth through cell division and thus formation of Stalk cells (Fig. 5*E*), thus not resulting in functional angiogenesis. Finally, we found that, phenotypically, the application of VEGF alone, without other components of the proangiogenic mixture with or without TNF (as initially analyzed in Fig. 2), was equivalent to the responses to the full proangiogenic mixtures with 10-fold lower VEGF concentrations (gray dots in Fig. 5*D*, and open symbols adjacent to points 4 and 6 in the diagram in Fig. 5*A*), suggesting that the components of the mixture act through the same molecular mechanisms in inducing angiogenic responses as those classically attributed to VEGF inputs, enhancing the VEGF signaling beyond what may be saturating levels. In the mathematical model, this case would correspond to a lower effective VEGF input.

We then experimentally examined the quantitative characteristics of the rescue effect of PCs on angiogenesis, at TNF levels above the threshold values and different VEGF concentrations (+PC in Fig. 5 *B*, *D*, and *E*). For both VEGF concentrations, at 100 ng/mL TNF (points 3′ and 6 in Fig. 5*A*), we observed a complete rescue of the angiogenesis, in a VEGF-dependent fashion, which was consistent with the model predictions. Strikingly, at the higher VEGF input (points 1 and 3′ in Fig. 5*A*), the effect of PCs was not only to rescue but to enhance the angiogenesis, leading to sprouts that were much longer (data indicated as +PC:1 and +PC:3 in Fig. 5 *B*, *D*, and *E*) than those observed for any of the VEGF/TNF combinations, in the absence of PCs. This effect was consistent with an increased formation of Stalk cells when PCs were present along with application of the highest levels of TNF and VEGF (Fig. 5*E*). A closer inspection of these sprouts revealed a high degree of variability in length and in the cell density (which was also associated with the sprout thickness) (Fig. 5*F*). We therefore explored whether this effect might be related to a variable PC coverage at the Tip/Stalk cell area during the sprout extension. We found that, for the condition shown as point 3 in Fig. 5*A*, a fraction of the sprouts was associated with a single PC cell at the sprout tip area. These sprouts were on average significantly longer and less dense (thinner) than the sprouts forming without a PC cell at the tip (Fig. 5*H*). However, PCs at the sprout tip area were only very rarely observed in the absence of TNF (Fig. 5*G*), resulting in a more variable sprout length and cell density distributions. These data suggested that the presence of a partial PC coverage at the threshold combination of VEGF and TNF (points 3, 3′ of Fig. 5*A*) can substantially improve the stability of the differentiation process, leading to more persistent migration and division phenotypes and thus longer sprouts. These data were again consistent with the mathematical model predictions, supporting the mechanism proposed here to explain the angiogenesis outcome at diverse combinations of TNF and VEGF inputs. Overall, our results suggested that a combination of diverse inputs of proangiogenic and antiangiogenic stimuli and PC coverage can strongly modulate the outcome of angiogenesis, resulting in wide range of shapes of incipient sprouts.

Discussion

The effect of the local inflammation and the associated cytokines on the onset and progression of angiogenesis is still a matter of debate (5, 7–9). In particular, it has been shown that, while TNF can show strong antiangiogenic effects (5, 7), it can also induce the Tip cell fate through up-regulation of a Notch ligand Jag-1, which might result in a proangiogenic function (8, 9, 26, 30). Here, through a combination of controlled experimentation with inducible angiogenesis in an engineered system and a computational model trained on the experimental data, we demonstrate that these apparently contradictory findings can be reconciled within a single framework. Furthermore, this framework accounts for diverse combinatorial effects of proangiogenic factors, such as VEGF, and proinflammatory cytokines, such as TNF, modulated by unanticipated juxtacrine influence of PCs. The mathematical model capturing the details of the signaling networks involved in specification of the Tip and Stalk cells predicted the existence of the critical TNF concentrations, above which the interactions between Dll4, Jag1, and Notch can no longer induce differentiation between neighboring ECs into distinct fates, yielding instead an intermediate or hybrid state. We also note that TNF, at high levels, may have an indirect effect on Notch signaling, by loosening cell junctions (31–34) and thus diminishing juxtacrine Notch receptor engagement. The lack of cell differentiation above a critical TNF level, in turn, abrogates successful sprout induction, since if a presumptive Tip cell is not supported by neighboring proliferative Stalk cells, it cannot successfully migrate into the surrounding matrix without severing its contacts with the other cells. This observation is consistent with our findings of stunted single-cell–sized minisprouts protruding from the parental vessel at TNF levels above the critical concentration. Likewise, if a Stalk fate induction is not supported by a neighboring Tip cell specification, the proliferative capacity inherent in the Stalk cell phenotype will be suppressed by the contact inhibition from neighboring cells within the endothelium due to the lack of Stalk cell separation from the rest of the monolayer. This is consistent with the apparent absence of Stalk cells at TNF concentrations above critical levels.

We found that PC coverage can rescue the inhibitory effect of TNF on angiogenesis, due to suppression of TNF signaling in ECs. Although the VEGF signaling in these cells is also inhibited by the juxtacrine effects of PCs, the influence of PCs on TNF signaling is more consequential, due to the properties of the thresholds, separating the proangiogenic and antiangiogenic effects of TNF. At almost all VEGF levels, the values of these thresholds are predicted to be effectively independent of the VEGF concentration. Therefore, suppressing VEGF signaling will have little effect on the critical TNF concentrations, although VEGF can modulate the

probability of induction of Tip and Stalk cells in a dose-dependent fashion, if angiogenesis proceeds (15).

The effects of PCs on angiogenesis are predicted to strongly depend on the PC coverage of ECs. This finding is important since PC coverage can vary across tissues, and between normal and cancerous vasculature, as well as be dynamic due to transient PC dissociation at the outset of angiogenesis (20, 35, 36). For a very low PC coverage, the effect of TNF is revealed to be fully inhibitory, if this cytokine exceeded the critical level. On the other hand, a high, uniform PCs coverage, affecting all ECs, can rescue the TNF-mediated suppression of angiogenesis, consistent with our experimental findings. The mathematical analysis suggests that, for an intermediate PC coverage levels, such that for many neighboring ECs only 1 cell in 2 would be in contact with a PC, the PC-mediated rescue of the inhibitory TNF effect can dramatically increase, essentially rendering TNF strongly proangiogenic. This effect, as predicted by the model, would occur due to an enhanced differentiation of neighboring ECs, guided by a higher TNF signaling in a cell that is not in contact with a PC and a lower signaling in a neighboring cell in contact with a PC. This asymmetry in signaling, coupled with the additional differentiation mediated by Notch signaling, can enhance the Tip/Stalk fate specification and promote the emergence and maturation of the nascent sprouts. This was consistent with the particularly pronounced growth and branching of the sprouts under conditions (high TNF levels) otherwise inhibitory to angiogenesis in the presence of PCs. Experimentally, in our assay, the PC distribution displayed local variations, and the predicted effect of partial PC coverage was supported by observation of specific sprouts, in addition to examining the average PC rescue effects. In particular, frequent observation of a PC at the tip areas of the particularly long sprouts, suggested that the Tip/Stalk fate selection may be stabilized by a combination of a partial PC coverage and TNF, not only during the onset of sprout extension but also during the sprout growth. Overall, our integrative analysis suggests an unexpected conclusion that angiogenesis can be particularly enhanced, leading to longer and more branched blood vessels, at relatively high ambient TNF levels in the presence of complete and partial coverage by PCs.

These findings are interesting to put into the context of the other commonly accepted views on the functions of PCs within the exiting vascular beds. Low and intermediate PC coverage has been suggested to result in lower stability and higher leakage of blood vessels, which might be an indication of either pathologic conditions (e.g., in the context of growing tumors) or dynamically reorganizing vasculature. This view is consistent with our observations, suggesting that high PC coverage can down-modulate the effects of TNF and possibly other relevant signaling inputs, thus protecting the cells from the environmental stimuli, which may otherwise decrease the stability of the vessel. The destabilizing effect of low PC coverage, on the other hand, can in part reflect a more variable effective sensitivity of ECs to various extracellular stimuli, leading to in appropriately extensive angiogenesis, which may result in suboptimal or altered functionality, unless PC coverage can be recovered through recruitment or differentiation of precursor cells.

In vivo, the local microenvironment can be highly dynamic. In particular, successful angiogenesis might lead to a gradual restoration of appropriate oxygen tension and also be accompanied by a progressive inflammation resolution. As these conditions evolve, the biochemical milieu may change along with dynamic alterations of inputs from mural cells, such as PCs, raising the question of how the resulting morphogenesis of vascular beds might be affected. Our analysis provides a useful framework that can help start analyzing the complex multifactorial control of this morphogenetic process critical in a variety of developmental and physiological settings. More generally, it can also provide an insight into how heterotypic cell interactions can also modulate Notch signaling in other contexts, regulating cellular differentiation outcomes.

Materials and Methods

The biomimetic 3D angiogenesis model consists of a polydimethylsiloxane chamber, an engineered blood vessel (diameter, 200 to 250 μm; length, 10 mm) embedded in collagen gel and a coverslip, and they were assembled without external jigs. By the serial steps of PC seeding, collagen gelation, and EC seeding as depicted in *SI Appendix*, Fig. S1, this method allows more controlled EC–PC layering. VEGF is applied on the hole to induce a gradient from the top to the endothelium channel, and TNF is directly injected through the endothelium channel as described in Fig. 1*C*. Newly formed sprouts were imaged with Leica scanning disk confocal microscope, and IMARIS (Bitplane) was used for quantifying the number and the length of sprouts. To unravel the interplay between Notch, VEGF, and TNF signaling pathways, we extended the mathematical model describing the interaction of Notch and VEGF developed by Boareto et al. (8) to account for the Notch–VEGF–TNF signaling network. The computational analysis was performed using the Python numerical library PyDSTool (37). The details of materials and methods can be found in *SI Appendix, Materials and Methods*. In addition, the model construction and parameters used for the model are discussed in *SI Appendix, Mathematical Modeling*.

ACKNOWLEDGMENTS. This work was supported by Grants NIH R01 GM072024 and U54 CA209992 (to A.L.); National Science Foundation (NSF) PHY-1605817 and Center for Theoretical Biological Physics, NSF PHY-1427654 (to H.L.); Marjory Meyer Hasselmann Fellowship (to F.B.); and Ramanujan Fellowship provided by Science and Engineering Research Board (SERB), Department of Science and Technology (DST), Government of India (SB/S2/RJN- 049/2018) (to M.K.J.). In addition, this work was supported by the Center for Theoretical Biological Physics sponsored by NSF Grant PHY-1427654 (to J.N.O.). J.N.O. is a Cancer Prevention and Research Institute of Texas (CPRIT) Scholar in Cancer Research. We acknowledge Anjelica L. Gonzalez, PhD, Yale University, for kindly sharing pericytes for this work.

1. R. H. Adams, K. Alitalo, Molecular regulation of angiogenesis and lymphangiogenesis. *Nat. Rev. Mol. Cell Biol.* **8**, 464–478 (2007).
2. M. Potente, H. Gerhardt, P. Carmeliet, Basic and therapeutic aspects of angiogenesis. *Cell* **146**, 873–887 (2011).
3. A. Albini, M. B. Sporn, The tumour microenvironment as a target for chemoprevention. *Nat. Rev. Cancer* **7**, 139–147 (2007).
4. S. A. Eming, T. Krieg, J. M. Davidson, Inflammation in wound repair: Molecular and cellular mechanisms. *J. Invest. Dermatol.* **127**, 514–525 (2007).
5. R. C. Sainson *et al.*, TNF primes endothelial cells for angiogenic sprouting by inducing a tip cell phenotype. *Blood* **111**, 4997–5007 (2008).
6. L. A. Madge, J. S. Pober, TNF signaling in vascular endothelial cells. *Exp. Mol. Pathol.* **70**, 317–325 (2001).
7. M. Fràter-Schröder, W. Risau, R. Hallmann, P. Gautschi, P. Böhlen, Tumor necrosis factor type alpha, a potent inhibitor of endothelial cell growth in vitro, is angiogenic in vivo. *Proc. Natl. Acad. Sci. U.S.A.* **84**, 5277–5281 (1987).
8. M. Boareto, M. K. Jolly, E. Ben-Jacob, J. N. Onuchic, Jagged mediates differences in normal and tumor angiogenesis by affecting tip-stalk fate decision. *Proc. Natl. Acad. Sci. U.S.A.* **112**, E3836–E3844 (2015).
9. R. Benedito *et al.*, The notch ligands Dll4 and Jagged1 have opposing effects on angiogenesis. *Cell* **137**, 1124–1135 (2009).
10. M. B. Chen *et al.*, On-chip human microvasculature assay for visualization and quantification of tumor cell extravasation dynamics. *Nat. Protoc.* **12**, 865–880 (2017).
11. D. H. Nguyen *et al.*, Biomimetic model to reconstitute angiogenic sprouting morphogenesis in vitro. *Proc. Natl. Acad. Sci. U.S.A.* **110**, 6712–6717 (2013).
12. K. J. Bayless, H. I. Kwak, S. C. Su, Investigating endothelial invasion and sprouting behavior in three-dimensional collagen matrices. *Nat. Protoc.* **4**, 1888–1898 (2009).
13. L. Jakobsson *et al.*, Endothelial cells dynamically compete for the tip cell position during angiogenic sprouting. *Nat. Cell Biol.* **12**, 943–953 (2010).
14. K. Bentley *et al.*, The role of differential VE-cadherin dynamics in cell rearrangement during angiogenesis. *Nat. Cell Biol.* **16**, 309–321 (2014).
15. D. P. Noren *et al.*, Endothelial cells decode VEGF-mediated Ca^{2+} signaling patterns to produce distinct functional responses. *Sci. Signal.* **9**, ra20 (2016).
16. H. M. Eilken, R. H. Adams, Dynamics of endothelial cell behavior in sprouting angiogenesis. *Curr. Opin. Cell Biol.* **22**, 617–625 (2010).
17. M. V. Hoang, M. C. Whelan, D. R. Senger, Rho activity critically and selectively regulates endothelial cell organization during angiogenesis. *Proc. Natl. Acad. Sci. U.S.A.* **101**, 1874–1879 (2004).
18. B. A. Bryan *et al.*, RhoA/ROCK signaling is essential for multiple aspects of VEGF-mediated angiogenesis. *FASEB J.* **24**, 3186–3195 (2010).

19. H. Gerhardt, C. Betsholtz, Endothelial-pericyte interactions in angiogenesis. *Cell Tissue Res.* **314**, 15–23 (2003).
20. G. Bergers, S. Song, The role of pericytes in blood-vessel formation and maintenance. *Neuro-oncol.* **7**, 452–464 (2005).
21. S. Alimperti *et al*., Three-dimensional biomimetic vascular model reveals a RhoA, Rac1, and N-cadherin balance in mural cell-endothelial cell-regulated barrier function. *Proc. Natl. Acad. Sci. U.S.A.* **114**, 8758–8763 (2017).
22. A. Herland *et al*., Distinct contributions of astrocytes and pericytes to neuroinflammation identified in a 3D human blood-brain barrier on a chip. *PLoS One* **11**, e0150360 (2016).
23. M. Campisi *et al*., 3D self-organized microvascular model of the human blood-brain barrier with endothelial cells, pericytes and astrocytes. *Biomaterials* **180**, 117–129 (2018).
24. J. Kim *et al*., Engineering of a biomimetic pericyte-covered 3D microvascular network. *PLoS One* **10**, e0133880 (2015).
25. E. Lee *et al*., A 3D in vitro pericyte-supported microvessel model: Visualisation and quantitative characterisation of multistep angiogenesis. *J. Mater. Chem. B Mater. Biol. Med.* **6**, 1085–1094 (2018).
26. D. A. Johnston, B. Dong, C. C. Hughes, TNF induction of jagged-1 in endothelial cells is NFkappaB-dependent. *Gene* **435**, 36–44 (2009).
27. G. Thurston, J. Kitajewski, VEGF and delta-notch: Interacting signalling pathways in tumour angiogenesis. *Br. J. Cancer* **99**, 1204–1209 (2008).
28. S. Selvam, T. Kumar, M. Fruttiger, Retinal vasculature development in health and disease. *Prog. Retin. Eye Res.* **63**, 1–19 (2018).
29. O. Shaya, D. Sprinzak, From Notch signaling to fine-grained patterning: Modeling meets experiments. *Curr. Opin. Genet. Dev.* **21**, 732–739 (2011).
30. J. Petrovic *et al*., Ligand-dependent Notch signaling strength orchestrates lateral induction and lateral inhibition in the developing inner ear. *Development* **141**, 2313–2324 (2014).
31. B. E. Dewi, T. Takasaki, I. Kurane, In vitro assessment of human endothelial cell permeability: Effects of inflammatory cytokines and dengue virus infection. *J. Virol. Methods* **121**, 171–180 (2004).
32. C. A. Aveleira, C. M. Lin, S. F. Abcouwer, A. F. Ambrósio, D. A. Antonetti, TNF-α signals through PKCζ/NF-κB to alter the tight junction complex and increase retinal endothelial cell permeability. *Diabetes* **59**, 2872–2882 (2010).
33. O. Shaya *et al*., Cell-cell contact area affects notch signaling and notch-dependent patterning. *Dev. Cell.* **40**, 505–511.e6 (2017).
34. P. R. Clark, R. K. Kim, J. S. Pober, M. S. Kluger, Tumor necrosis factor disrupts claudin-5 endothelial tight junction barriers in two distinct NF-κB-dependent phases. *PLoS One* **10**, e0120075 (2015).
35. L. Zhang *et al*., Presence of retinal pericyte-reactive autoantibodies in diabetic retinopathy patients. *Sci. Rep.* **6**, 20341 (2016).
36. F. J. Huang *et al*., Pericyte deficiencies lead to aberrant tumor vascularizaton in the brain of the NG2 null mouse. *Dev. Biol.* **344**, 1035–1046 (2010).
37. R. Clewley, Hybrid models and biological model reduction with PyDSTool. *PLoS Comput. Biol.* **8**, e1002628 (2012).